AMERICAN SOCIETY FOR MICROBIOLOGY | Journal of Bacteriology

Population Dynamics of Phage and Bacteria in Spatially Structured Habitats Using Phage λ and *Escherichia coli*

Namiko Mitarai, Stanley Brown, Kim Sneppen

Center for Models of Life, Niels Bohr Institute, University of Copenhagen, Copenhagen, Denmark

ABSTRACT

Bacteria living in physically structured habitats are exposed heterogeneously to both resources and different types of phages. While there have been numerous experimental approaches to examine spatially distributed bacteria exposed to phages, there is little theory to guide the design of these experiments, interpret their results, or expand the inferences drawn to a broader ecological and evolutionary context. Plaque formation provides a window into understanding phage-bacterium interactions in physically structured populations, including surfaces, semisolids, and biofilms. We develop models to address the plaque dynamics for a temperate phage and its virulent mutants. The models are compared with phage λ-*Escherichia coli* system to quantify their applicability. We found that temperate phages gave an increasing number of gradually smaller colonies as the distance increased from the plaque center. For low-lysogen frequency this resulted in plaques with most of the visible colonies at an intermediate distance between the center and periphery. Using spot inoculation, where phages in excess of bacteria were inoculated in a circular area, we measured the frequency and spatial distribution of lysogens. The spot morphology of *c*II-negative (*c*II$^-$) and *c*III$^-$ mutants of phage λ displays concentric rings of high-density lysogenic colonies. The simplest of these ring morphologies was reproduced by including multiplicity of infection (MOI) sensitivity in lysis-lysogeny decisions, but its failure to explain the occasional observation of multiple rings in *c*III$^-$ mutant phages highlights unknown features of this phage. Our findings demonstrated advantages of temperate phages over virulent phages in exploiting limited resources in spatially distributed microbial populations.

IMPORTANCE

Phages are the most abundant organisms on earth, and yet little is known about how phages and bacterial hosts are influencing each other in density and evolution. Phages can be either virulent or temperate, a difference that is highlighted when a spatially structured bacterial population is infected. Phage λ is a temperate phage, with a capacity for dormancy that can be modified by single gene knockouts. The stochastic bias in the lysis-lysogeny decision's probability is reflected in plaque morphologies on bacterial lawns. We present a model for plaque morphology of both virulent and temperate phages, taking into account the underlying survival of bacterial microcolonies. It reproduces known plaque morphologies and speaks to advantages of temperate phages in a spatially structured environment.

The active biomass on earth is dominated by prokaryotes, which constitute about half the amount of the carbon stored in living organisms (1). Bacteria are widely exposed to phages, which in turn are the most numerous inhabitants of our biosphere (2, 3). Phages have developed a diversity of behaviors that support their survival (survival strategies), which continues to inform our understanding of evolution and gene editing (4–8). One classical phage type consists of temperate phages (9), in which infecting phages choose lysogeny, a condition in which they will remain over many bacterial cell generations. This is predicted to facilitate long-term survival when phages are faced with variability in bacterial host density (10, 11). Furthermore, phages are found to be major carriers of genes between prokaryotes (12), including pathogens. For example, a number of toxin genes are phage borne: the cholera toxin gene in *Vibrio cholerae* (13–15), the diphtheria toxin in *Corynebacterium diphtheriae* (16, 17), the gene for toxic shock syndrome toxin 1 in *Staphylococcus aureus* (18), and Shiga toxins in the enterohemorrhagic strains of *Escherichia coli* (15, 19).

Many of the theoretical works on phage-bacterium interactions have assumed well-mixed populations (20–24). Even though they provide tremendous insights, such assumptions may predict quite unstable population fluctuations, while even in chemostat experiments the population fluctuations are an order of magnitude less than predicted (21). Possible remedies for this discrepancy between theory and experiments could include heterogeneous bacterial phenotypes (25, 26) or spatial inhomogeneity. Supporting the latter, it has been experimentally demonstrated that limited migration can promote coexistence (27). Cellular automaton-type models have been used to address the spatial effect in phage-bacterium interactions (27, 28), but their coarse description of bacterial colonies limited their applicability to qualitative predictions. These concerns could be addressed with a model that can quantitatively analyze phage-bacterium interactions in spatially structured populations.

Plaque morphology is a classical tool to investigate and quan-

Received 5 December 2015 **Accepted** 5 April 2016

Accepted manuscript posted online 11 April 2016

Citation Mitarai N, Brown S, Sneppen K. 2016. Population dynamics of phage and bacteria in spatially structured habitats using phage λ and *Escherichia coli*. J Bacteriol 198:1783–1793. doi:10.1128/JB.00965-15.

Editor: T. J. Silhavy, Princeton University

Address correspondence to Namiko Mitarai, mitarai@nbi.dk.

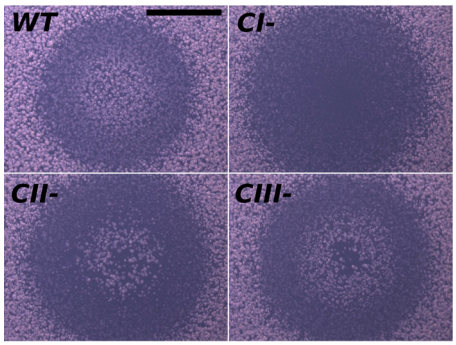

FIG 1 Plaque morphology caused by a single initial phage. The progeny spread on a bacterial lawn with a relatively low initial density of bacteria. The four panels reflect the final patterns obtained about 12 h after an initial infection of a wild-type λ and mutants that lack one of the central factors in the lysis-lysogeny decision circuit (29, 59–62). wt is wild-type λ phage displaying a classical turbid plaque, whereas the *c*I$^-$ mutant gives a clear plaque. The two mutants shown in the lower panels give weaker turbid plaques, with additional spatial features. Scale bar, 1 mm. For the influence of mutants on the λ phage regulatory network see, e.g., the work of Avlund et al. and Trusina et al. (56, 63).

tify phage behavior (29, 30) and is the simplest model system to investigate spatially structured systems exposed to bacterium-phage interaction. A low number of phages are mixed with a much higher number of bacteria in a soft agar, cast in a thin layer on a hard agar plate, and subsequently incubated overnight (double-agar overlay method) (30). When this is done with the temperate phage λ and *E. coli*, the phages infect and spread until the bacteria have entered the stationary phase. The final stationary plaque is then surrounded by a dense lawn of bacterial colonies, as illustrated in Fig. 1. The plaque morphology depends on the ability of the phage to infect the bacteria as well as on the probability that infecting phages enter lysogeny. When a lysogen is formed, it is immune to further infections and subsequently grows to a microcolony with a size that depends on the remaining resource availability.

Analyses of phage growth in liquid medium and in soft agar overlays are complementary. Plaque formation in soft agar has led to the genetic identification of regulatory networks (29, 31). Alterations in plaque or spot morphologies reflect alterations in regulation and function of phage genes. By spatially separating the infection events, plaque assays allow the resources to be consumed locally, preventing phage growth from being dominated by a single phage or host survivor. On the other hand, studies of phage growth in liquid medium have unraveled the physiology of the same regulatory networks (32–34). More detailed analyses of plaque formation may improve our understanding of the decision processes occurring during phage infection, and the derived models may suggest new plaque morphologies to seek in genetic analyses of phage growth.

Figure 1 shows plaques of phage λ and some of its mutants. The wild-type (wt) plaque illustrates a classical turbid plaque, where each white colony in the center consists of lysogens and where the darker ring surrounding it contains both older colonies that are being reduced by phage predation and young small and invisible colonies of lysogenic bacteria.

In Fig. 1, the image of the *c*I-negative (*c*I$^-$) mutant shows how a λ mutant that can only kill its host effectively clears all bacteria in the center of the plaque. In this panel remnants of bacterial colonies are also observed near the periphery of the plaque. This shows that even at abundant density phage did not instantly kill all bacteria and therefore that bacteria in a large colony suspended in soft agar may only slowly be lysed during the phage attack.

The bottom panels in Fig. 1 show two mutants of phage λ with a reduced but finite ability to form lysogens (32, 33). The *c*II$^-$ mutant has lost the transcriptional activator CII and, as a consequence, has less production of the lysogen maintenance protein CI during infection (35). This reduces the frequency of lysogens, and in the panel showing the *c*II$^-$ mutant, only a few colonies were observed in the central region of the plaque. It is noticeable that these surviving colonies were less inhibited by resource competition from other colonies and grew to larger sizes than lysogens in the wt panel. The *c*III$^-$ mutants are believed to have reduced activity of CII (36) and as a result display an intermediate level of surviving colonies in the plaque. It is also noticeable that in the images of the both *c*II$^-$ and *c*III$^-$ mutants, there is a pronounced "hole" in the center, surrounded by a ring of lysogens. This hole represents the absence of lysogeny during the early infection cycles of the phage.

In spite of the widespread usage of plaque assays, quantitative studies that address the relationship between the phage properties and the plaque morphology are few. Most of them focus on virulent phages and formation of clear plaques. The experimental work by Hendrix and Duda (37) and more recently by Gallet et al. (38) used various λ phages mutant in their tail fibers to address the effects on the plaque expansion speed and plaque size. Most modeling studies examine the plaque enlargement at a constant speed in a lawn of constant bacterial density, as seen with virulent phage T7 (39–44). Kaplan et al. (45) assumed a constant bacterial growth rate and a final time given by geometrical constraint to determine final plaque sizes. However, many phages, including λ, can form plaques only when the medium allows the bacteria to be metabolically active and cannot propagate in a stationary-phase lawn. For temperate phages, plaque morphology has been abundantly described experimentally (29, 30), but we have been unable to find any quantitative model.

Here, we present a reaction-diffusion-based model for plaques formed by temperate phages, which allows us to analyze the phage plaques. In particular, we focus on the parts of the plaque that are caused by lysogens, which show interesting structures due to the stochastic nature of the lysogenization. We also provide a method to interpret the result in terms of microcolony size and distribution to reconstruct an image that can be visually compared to experimentally obtained plaques. The comparison allowed us to address the relation between the morphology of the plaque and phage properties.

MATERIALS AND METHODS

Experimental protocol. (i) Plaque assay. The host strain for all experiments was S1754tonA (F$^-$ *lacI*^{q} *metA endA hsdR17 glnV44 thi1 relA1 gyrA96 fhuA*) (46). Phage were λ$^+$ (a gift from T. Silhavy), λ*c*II*sus41* (*sus41* is an amber mutation in *c*II that is poorly suppressed by *glnV* [47]) (laboratory collection), λ*c*III67 (31) (laboratory collection), and λ*c*Ib221 (a gift from J. Beckwith).

Bacterial cultures for all experiments were grown in yeast extract-tryptone (YT) broth (48) at 37°C. Cultures used for visualizing plaques were pregrown in medium supplemented with 0.2% (wt/vol) maltose. Cultures used for phage spot tests (31) were supplemented with 0.2% (wt/vol) maltose if cast on agar supplemented with maltose. Cultures and

adsorption mixes were cast as soft-agar overlays in F-top agar (48) supplemented with 10 mM $MgCl_2$. The bottom agar was T-agar (48) supplemented with 0.1% (wt/vol) yeast extract (47).

If indicated in the respective figure legend, the bottom agar was supplemented with 0.2% (wt/vol) maltose. Phage lysates were diluted with thiomethylgalactoside (TMG) (49) before use. Plates were incubated at 37°C. The extent of phage spots was visualized by supplementing the dilutions of phage lysates with rhodamine-labeled beads. Dynabeads M-270 with amine (Invitrogen) were labeled with Lissamine rhodamine B-sulfonyl chloride (Molecular Probes) as per the manufacturer's instructions. Micrographs of phage growth were obtained using dark-field illumination. Rhodamine-labeled beads were visualized with fluorescent illumination.

(ii) Lysogenic state in spots. Spots of λ *c*II or *c*III were prepared as described above and incubated overnight. The next day, six samples were picked with round toothpicks from either the rings or the central region, and bacteria were purified by streaking on YT agar. Purified colonies were tested (one colony per pick) for lysogenic state by cross-streaking against phages λ*c*Ib221 and λ*vir*.

Model. We describe the system using a two-dimensional partial differential equation for the densities at position **r** at time t of the sensitive bacteria, $B(\mathbf{r}, t)$, the lysogens, $L(\mathbf{r}, t)$, the phage, $P(\mathbf{r}, t)$, and the nutrient, $n(\mathbf{r}, t)$. We assume that the system is uniform in the depth direction of the soft agar, which has thickness Δa. We assume that the bacterial cells do not move or diffuse; under the condition used here, the bacteria appear immobile, as manifested in the sharp edge of microcolonies. The phage and the nutrient are assumed to diffuse in space. The bacterial density obeys the following equation:

$$\frac{\partial B}{\partial t} = g(n) \cdot B - \frac{\eta}{\Delta a} \cdot P \cdot B \tag{1}$$

where we assume the Monod growth law for the bacterial growth rate $g(n)$ as:

$$g(n) = g_{\max} \cdot \frac{n}{n + K} \tag{2}$$

with the maximum growth rate, $g_{\max}$, being 1/(30 min) for *E. coli* [corresponding to a doubling time of 1/(30 min)/ln(2) ≈ 20 min]. The important role of the nutrient, n, in this model is that it limits the bacterial growth rate; thus it can represent the amount of limiting factor in the medium, not necessarily a carbon source.

The second term in equation 1 represents the phage infection, parameterized by the phage adsorption rate, η. It is divided by the soft-agar thickness, reflecting that we do not take into account spatial structures along this direction.

(i) Model without MOI dependence in the lysis-lysogeny decision. In the simplest case where the lysis-lysogeny decision is independent of the multiplicity of infection (MOI), the infected bacterium is assigned a direct lysogen probability, α. This probability may well depend on the bacterial growth rate, but we keep it constant in most of our simulations. The lysogens become immune to reinfection by the phage. This leads to the following equation for lysogen density:

$$\frac{\partial L}{\partial t} = \alpha \frac{\eta}{\Delta a} \cdot P \cdot B + g(n) L \tag{3}$$

When the lytic pathway is chosen (with a probability of 1 − α per infection), the phage replicates inside the infected bacterium. The rate for the phage replication is expected to be proportional to the growth rate of the bacterium. Some investigators have modeled the phage replication process as a burst with an explicit time delay (43, 44), but here we take the effective delay into account by assuming 10-step sequential reaction processes between the infection and the burst, with the identical transition rates to the next the steps. Having intermediate steps allows variation in the latency period. The multistep model narrows the distribution of the latency period for the phage burst compared to that of the one-step model (41, 42), which would give an exponential distribution for the latency period. The 10-step reaction processes corresponds to about 30% ($1/\sqrt{10}$) cell-to-cell spread in the time to lysis.

The ith step of the infected bacterial density, I_i, obeys the following:

$$\frac{\partial I_1}{\partial t} = (1 - \alpha) \frac{\eta}{\Delta a} \cdot P \cdot B - \frac{10}{1.5} \cdot g(n) \cdot I_1 \tag{4}$$

$$\frac{\partial I_i}{\partial t} = \frac{10}{1.5} \cdot g(n) \cdot (I_{i-1} - I_i) \text{ (for } i = 2, \ldots 10) \tag{5}$$

Here, we assume that the latency period for the phage burst is inversely proportional to the bacterial growth rate. The transition rate, $(10/1.5) \cdot g(n)$, between the 10 infection steps gives the average latency period to be $1.5/g(n)$. This is consistent with the measured latency period of 42 min for wt λ in mid-log phase of growth at 37°C on LB medium (50), with a doubling time of $\ln(2)/g(n) \approx 20$ min. After latency the bacterium lyses to release β progeny phages, where β is the burst size of the phage replication:

$$\frac{\partial P}{\partial t} = \beta \cdot \frac{10}{1.5} \cdot g(n) \cdot I_{10} + D_P \nabla^2 P - \frac{\eta}{\Delta a} \cdot P \cdot \left(B + \sum_{i=1}^{10} I_i + L \right) - \delta \cdot P \tag{6}$$

Here, the first term represents the phage burst, the second term denotes the phage diffusion with constant D_P, and the last term represents the loss of free phage by adsorption to the bacteria. The phage decay rate, δ, has a time scale of days (50), and hence its effect is negligible in the present study.

Finally, the nutrient is consumed by the bacterial growth and also diffuses with constant D_n, giving

$$\frac{\partial n}{\partial t} = -g(n) \cdot (B + L) + D_n \nabla^2 n \tag{7}$$

Here, we measure the nutrient density in the unit that permits one bacterium to divide, creating one new cell. Therefore, the yield coefficient in the first term of the above equation is equal to 1.

(ii) Model with MOI dependence in the lysis-lysogeny decision. We also modeled the case where the lysis-lysogeny decision depends on the MOI (see Results for details). Based on the MOI dependence for wt λ phage measured by Kourilsky and Knapp (32, 33), who observed that lysogen frequency is significant only with an MOI of >1 (two or more phages infect the same bacterium in the same small time window before the decision is made), in this model we assume that a phage always chooses lysis for a single infection, but if more infections occur within 1/10 of the latent time, the phage enters lysogeny with probability αfor each additional infection. In this case, we modify equation 4 for the first infection step I_1 to be

$$\frac{\partial I_1}{\partial t} = \frac{\eta}{\Delta a} \cdot P \cdot B - \alpha \cdot \frac{\eta}{\Delta a} \cdot P \cdot I_1 - \frac{10}{1.5} \cdot g(n) \cdot I_1 \tag{8}$$

and the lysogen density develops by

$$\frac{\partial L}{\partial t} = \alpha \frac{\eta}{\Delta a} \cdot P \cdot I_1 \cdot + g(n) L \tag{9}$$

where the last term takes into account the growth of earlier formed lysogens.

(iii) Boundary condition and initial condition. The partial differential equations are solved in polar coordinates with the origin at the center of a plaque. This confines us to circular plaques, and spatial variation is only considered along the radial direction, r. At a distant outer boundary, $r = R_{\max}$, we impose reflecting boundary conditions for both phage and nutrient density.

Initially, bacteria and nutrient are uniformly distributed [$B(r, 0) = B_0$ and $n(r, 0) = n_0$], and there are no lysogens [$L(r, 0) = 0$]. For the plaque simulation by single infection, one infected bacterium is placed in the middle [$I_1(r, 0) = \delta(r)$, with $\delta(x)$ being the Dirac delta function], and there are no free phage [$P(r, 0) = 0$]. For the spot inoculation (see below),

TABLE 1 Default parameters used in the simulation[a]

Symbol	Meaning	Default value(s)	Comment and/or reference(s)
R_{max}	Radius of the simulated system	10 mm	Large compared to plaques
r_{spot}	Radius of the spot	2 mm	Only for spot simulation
Δa	Thickness of the soft agar	0.5 mm	Experimental setup in this study
n_0	Initial nutrient concn (unit of corresponding bacterial cells/area)	30/μm^2	Experimental setup in this study (evaluated from measured colony size and counts)
K	Michaelis-Menten constant for Monod growth law	$n_0/5$	Implies slowdown of growth when 20% of final density is reached
D_p	Phage diffusion constant	4×10^4 μm^2/h (~10 μm^2/s)	For λ in water (6 μm^2/s [53] or 18 μm^2/s [64])
η	Phage adsorption rate	8×10^4 μm^3/h (~1×10^{-9} ml/min)	Compare references 38 and 50
δ	Phage decay rate	0.003/h	50
g_{max}	Maximal growth rate	2/h	
β	Phage burst size	100	50
D_n	Diffusion constant of nutrient	4×10^5 μm^2/h (~100 μm^2/s)	Compare 200 μm^2/s (51) and ~1,000 μm^2/s (52) for small-molecule diffusion in agar

[a] Experimentally used lawns typically have one bacterium per 36 μm^2 or one bacterium per 320 μm^2.

we use a constant phage density for a limited range [$P(r, 0) = P_0$ for $r \leq r_{spot}$; otherwise $P(r, 0) = 0$].

(iv) Numerical integration. The equations are solved by the finite difference method. The size of the spatial discretization, Δr, for the integration is chosen such that there is one bacterium per Δr^2 at the initial condition (i.e., $\Delta r^2 = 1/B_0$). The time integration is done by the Euler method with a time step of $10^{-6}/g_{max}$, and the simulation is terminated at 20 bacterial generations ($t_{final} = 20/g_{max}$). The Fortran code is available upon request. We note that the numerical solution of partial differential equations may harbor more pitfalls than the numerical solution of ordinary differential equations.

(v) Parameter values. The default parameters are summarized in Table 1. The nutrient diffusion constant is assumed to be somewhat lower than the literature values (51, 52) in order to reproduce the observation that the final bacterial biomass in the center of each of the three spot assays is the about same and thus independent of the number of locally surviving colonies (see Fig. 5).

It should also be noted that the adsorption rate η is a difficult parameter to infer from the literature since (i) the phage receptor density depends strongly on the growth condition (53) and (ii) the available measurements do not distinguish between phages that successfully completed infection and phages attached to the bacterial wall but not committed to infect. Here, we varied the adsorption rate by an order of magnitude and found that the reported results were only moderately sensitive to the value of η.

The initial densities of bacteria, B_0, and, in the case of spots, of phages, P_0, are chosen to match with those of the corresponding experiment. The lysogenic probability αis fitted to match the colony counts in the spot experiments when appropriate, as explained in Results.

(vi) Reconstruction of the microcolony distribution. We reconstruct the image of the microcolony distribution in plaques from the density profiles produced by the model. To do this, we need to take into account the stochastic nature of the lysogeny decision. This can be done by noting that initially there is only one bacterium per area of $\Delta r^2 = 1/B_0$. The reconstruction consists in calculating the chance that this bacterium gives rise to a final microcolony and, in that case, how big this colony becomes. The detailed algorithm is given in the following.

(vii) Algorithm for reconstruction of the microcolony distribution. In the simulation, we know how much lysogen decision, $\Delta L_d(r, t)$, is made per area Δr^2 per short time duration from t to $t + \Delta t$. It is obtained by

$$\Delta L_d(r, t) = \Delta r^2 \int_t^{t+\Delta t} \alpha \frac{\eta}{\Delta a} \cdot P \cdot B dt \quad (10)$$

for the condition without MOI dependence in equation 3 and

$$\Delta L_d(r, t) = \Delta r^2 \int_t^{t+\Delta t} \alpha \frac{\eta}{\Delta a} \cdot P \cdot I_1 dt \quad (11)$$

for the MOI-dependent case of equation 9. For small enough Δt, $\Delta L_d(r, t)$ gives the probability to get a new lysogen decision per microcolony per Δt, allowing us to make stochastic interpretation of the model.

In practice we need to take finite Δt, and then sometimes $\Delta L_d(r, t)$ may exceed 1 if bacterial population B per microcolony is large enough. If so, we use the binomial distribution to estimate the number of newly converted lysogens in this colony. We then evaluate the final lysogen population size for each colony by allowing newly formed lysogens to grow with the growth rate $g(n(r, t))$ using the nutrient level, $n(r, t)$, calculated in the simulation. The final colony size is obtained by summing contributions from all lysogens. The final contributions of the sensitive and infected bacterial cells for each microcolony are also added to the final microcolony size.

The explicit algorithm is the following for the MOI-independent case.

1. Record the decision to go lysogen, $\Delta L_d(r, t)$, the nutrient level, $n(r, t)$, and the sensitive bacterial population, $B(r, t)$, per microcolony (i.e., per discretized lattice size with width Δr) per time step Δt, which was chosen to be $10^{-2}/g_{max}$.
2. Calculate the total number of bacteria at time zero, N_0, for the entire image with area A as $N_0 = B_0 A$. Thus, each box of $A/N_0 = 1/B_0$ will have, on average, one initial bacterium.
3. Repeat the following steps for each of the N_0 initial microcolonies.
   A. Choose a random position (x, y) in the given area from a uniform distribution.
   B. Calculate $r = \sqrt{x^2 + y^2}$.
   C. Set the number of lysogens in the microcolony at time zero to be $l = 0$, and do the following procedure from time zero to t_{final} in steps of Δt.
      i. If $\Delta L_d(r, t) < 1$, then increase number of lysogens at the location l by one with a probability $\Delta L_d(r, t)$.
      ii. If $\Delta L_d(r, t) > 1$, then calculate $p = \Delta L_d(r, t)/B(r, t - \Delta t)$ as the probability per cell for this time step that a cell will go lysogenic. Calculate the number of cells that went lysogenic at this time step from the binomial distribution with probability p and the total number of cells, $\lfloor B(r, t - \Delta t) \rfloor$ (rounded off to the nearest integer). Add this number to l.
      iii. Let the l lysogen cells grow over time based on the recorded nutrient level.
   D. Calculate the final radius of the surviving microcolony r_m from the final size l summed with surviving sensitive bacteria $B(r, t_{final})$ and infected bacteria $I \equiv \sum_{i=1}^{10} I_i(r, t_{final})$ at the corresponding

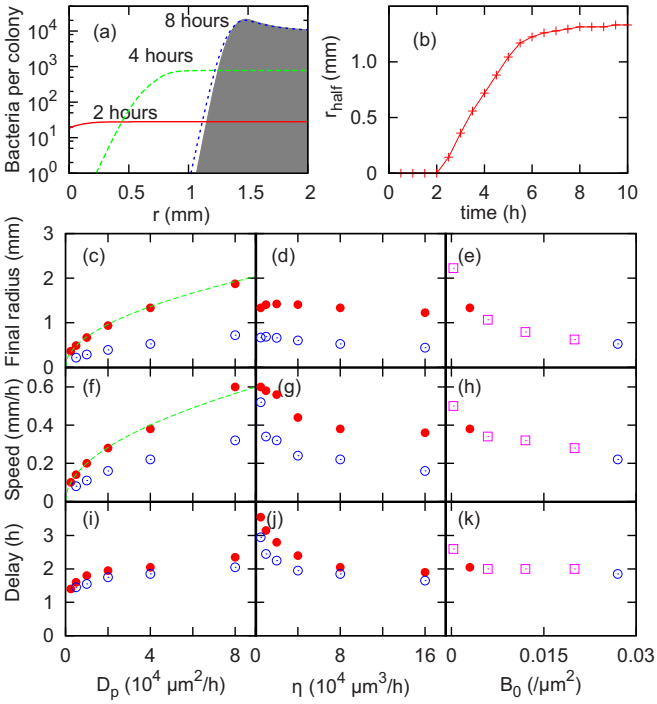

FIG 2 Simulation of plaque dynamics caused by a single virulent phage. (a) The development of the bacterial density with the default parameter set and initial bacterial density $B_0 = 1/(320\ \mu m^2)$. The gray region shows the final number of bacteria per microcolony as a function of the distance from the infection center r. We define the plaque radius, r_{half}, as a position at which the bacterial concentration is half of that at large distances. (b) The development of the plaque radius, r_{half}, from the simulation shown in panel a. The bottom panels show the final plaque radius (c to e), the plaque expansion speed dr_{half}/dt (f to h), and the plaque appearance delay time (time at which r_{half} start to increase from zero) (i to k) as a function of phage/bacterial parameters. For each plot, all parameter but the varied parameter are kept at their default values. The filled circles are the data with $B_0 = 1/(320\mu m^2)$, and the open circles are those with $B_0 = 1/(36\ \mu m^2)$. For the dependence on phage diffusion rate D_p (c and f), we also show dashed lines that are proportional to $\sqrt{D_p}$.

position. We assume that a microcolony is a dense sphere of bacteria with one bacterium occupying a volume of 1 μm^3; therefore we have $\frac{4}{3}\pi r_m^3 = l + I + B(r, t_{final})$.

E. Draw a circle of radius r_m centered at (x, y) as a final microcolony.

For the MOI-dependent case, $B(r, t)$ in procedure steps 1 and 3C should be replaced with $I_1(r, t)$ to reflect that the lysogens come only from already infected bacteria.

RESULTS

Plaque formed by single virulent phage infection. We first summarize the predicted expansion dynamics and the final plaque size for virulent phage infection by setting the lysogen-probability α to be zero. This situation corresponds to the plaque formation in nonlysogenic *E. coli* hosts by a *c*I$^-$ mutant phage, which effectively behaves as a virulent phage. Figure 2a shows growth of the bacterial lawn along with the plaque formation starting at $r = 0$ at time zero with the default parameters adjusted to a *c*I$^-$ mutant of phage λ. After ~8 h, the bacterial lawn stops growing due to depletion of the growth medium. We define the plaque radius r_{half} where the bacterial density is half of that found in the undisturbed lawn. The dynamics of r_{half} is shown in Fig. 2b. After some delay, r_{half} increases almost linearly over time (2 to 5 h). Thereafter it slows down, stopping at around 8 h.

From the plot of r_{half} (Fig. 2b), we define the final plaque radius as r_{half} at 10 h, and we define the expansion speed by the increase of r_{half} at the beginning of the linear expansion. The delay time for the plaque appearance is defined as time at which r_{half} starts to increase from zero. These quantities are explored in Fig. 2c to k. When the phage diffusion constant D_p is varied, both the final radius (Fig. 2c) and the speed (Fig. 2d) changed proportionally to $\sqrt{D_p}$. This form of speed dependence was also predicted for expansion of a plaque on a stationary lawn (39–44). The dependence of plaque size on the adsorption rate is rather weak (Fig. 2e), consistent with previous experimental observations (38). The initial bacterial density, B_0, influences both the expansion and the final size because the bacteria absorb large amounts of phages and because a large initial density limits the time before nutrient depletion influences the growth.

Plaque formed by single temperate phage infection. A temperate phage does not always kill its host but can instead choose lysogeny and, in the case of λ, integrate its genome into the bacterial chromosome, where it will protect the bacterium from further infections. The lysogenic probability α is not just a fixed number for a given phage but will depend on conditions. The lysis-lysogeny decision in wt λ is, for example, dependent on the multiplicity of infection (MOI) (32, 33). For an MOI of 1 (only one phage infects the bacterium), the phage nearly always chooses lysis, whereas infections with an MOI of >1 (two or more phages infect the same bacterium in the same small time window before the decision is made) allow a substantial fraction to choose lysogeny (54–57).

In addition, the lysogenic pathway is favored by slower growth of the host (32, 33), which in turn suggests that lysogens should be increasingly favored in the late stages of plaque development. For the *c*II$^-$ and *c*III$^-$ mutants, their decision is biased toward lysis compared to that of the wt, but it is unclear whether they have any MOI dependence. Kourilsky and Knapp (33) report that *c*III$^-$ mutants have sensitivity to average phage input (API; the ratio of the number of available phage particles to the number of bacteria) when infections are done together with a low density of c^+ phages.

We therefore simulate the situation with and without MOI dependence, as well as with various values of α. The case without MOI dependence is modeled by taking the lysis-lysogeny decision at the first infection with a probability of α and preventing further infections from altering the decision. For the case with MOI dependence, our model assumes that the first infection takes the bacterium into an infected state, and if further infections occur within the allotted time window, then the bacterium switches to form a lysogen with a probability of αfor every additional infection (see "Model" above).

Figure 3 shows simulated plaque morphologies from single temperate phage infections. The blue, gray, and red areas mark microcolonies consisting of the phage-sensitive (B), infected (I), and lysogenic (L) bacteria, respectively. The difference in lysogenic probability α is reflected in the density of lysogen microcolonies (compare Fig. 3a [where α = 0.1] and c [where α = 0.005] for the case without MOI dependence or b [where α = 0.1] and d [where α = 0.005] for the case with MOI dependence). Noticeably, the MOI dependence does not give a qualitative difference in the morphology (compare Fig. 3a and b or c and d).

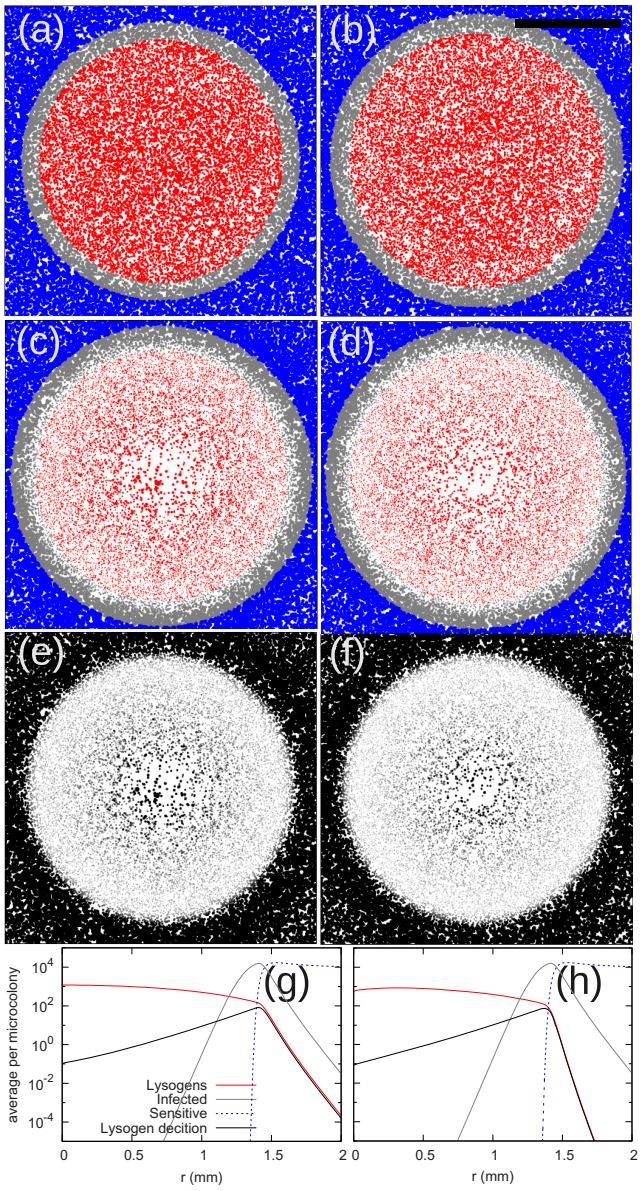

FIG 3 Simulations of plaques formed by a single temperate phage infection. Default parameters were used for a lawn with initial density $B_0 = 1/(320\ \mu m^2)$, here shown after 10 h of incubation. The width of the shown area is 3 mm. Scale bar, 1 mm. (a) Simulation with no MOI dependence and $\alpha = 0.1$. The microcolonies dominated by sensitive bacteria are shown as blue, lysogens are red, and gray marks cells in latency. The same color code applies to panels b to d. (b) Simulation with MOI dependence and $\alpha = 0.1$. (c) Simulation with no MOI dependence and $\alpha = 0.005$. (d) Simulation with MOI dependence and $\alpha = 0.005$. (e) Simulation with no MOI dependence and $\alpha = 0.005$ as in panel c, where the colonies smaller than 10 μm in radius are displayed in a lighter shade of gray in proportion to their radius. (f) Simulation with MOI dependence and $\alpha = 0.005$ The visualization method is the same as that in panel e. (g) Profiles of lysogens, sensitive cells, infected cells, and the number of cells that directly took the lysogen decision (cumulative sum over time) for the simulations with no MOI dependence and $\alpha = 0.005$. (h) Profiles as described for panel g but for the simulations with MOI dependence and $\alpha = 0.005$.

Figure 3a to d predict plaques which are more uniformly turbid than the real plaques shown in Fig. 1. Thus, we predict that there should be many surviving lysogens near the periphery of the plaque but also that these lysogens are in small microcolonies below the visible detection threshold. Figure 3a to d display all microcolonies irrespective of their size. Mimicking the visibility of colonies by making smaller microcolonies dimmer, one obtains the images shown in Fig. 3e and f that resemble overall features shown Fig. 1: the plaques exhibit a central region of high density of visible lysogens, surrounded by a dark region with nearly no visible life. However, we stress that the major part of this structure is visual and that there indeed are survivors also in the dark region.

Another remarkable feature is depletion in the middle of some of the plaques shown in Fig. 1. Noticeably, such a hole can be obtained with or without MOI dependence, as long as α is not too high (Fig. 3e and f), and quantitatively this appears as fewer lysogen decisions in the center of the plaque (Fig. 3g and h). The hole appears at the first or second round of phage bursts, which eliminate bacteria in the center before they multiply. Later, when each bacterium has formed an initial microcolony, only one member of each colony needs to survive to provide a final microcolony.

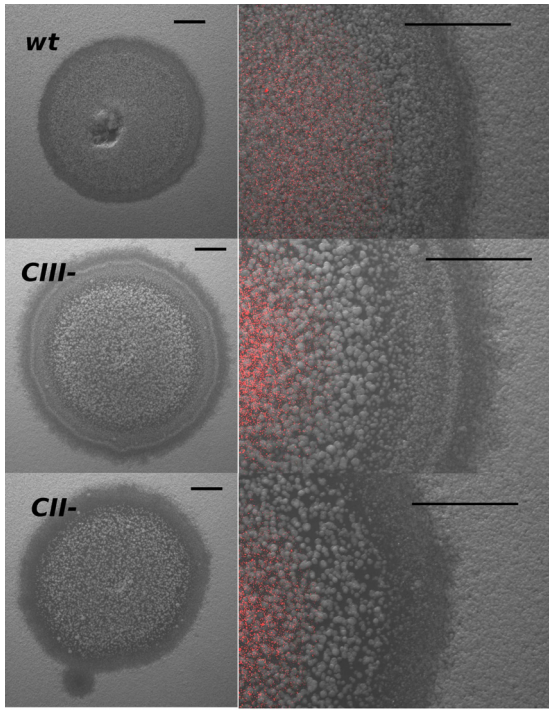

FIG 4 Morphology of spots obtained by spot assay. The plaques are formed by initial addition of a droplet of water with phages, progeny of which spread on the growing bacterial lawn. The bottom agar was supplemented with maltose. The rightmost panels show part of the plaque at higher magnification and with red beads that mark the initial distribution of phages. The estimated initial conditions represent bacterial density $B_0 = 1/(36\ \mu m^2)$ and phage density $P_0 = 1/(18\ \mu m^2)$. Thus, API within the droplet is 3 for the wt and 2 for the cII^- and cII^- mutants. Scale bar, 1 mm.

Spot assay. For characterization of phages, one may in addition consider a spot assay (31). In this method, a droplet of water with many phages is placed on a soft-agar overlay seeded with bacteria, and the spot is studied after overnight incubation (see Materials and Methods). As seen from Fig. 4 this assay showed clear differences between the studied phage mutants.

Figure 4 shows spots with a relatively high density of bacteria and phages, giving the API at the spot $P_0/B_0 = 2$. Note that the API is different from the MOI due to the stochastic infection process:

some bacteria are infected by more phages than the API, and some are infected by fewer phages. Also one would expect that some phages diffused into the bottom agar. Simultaneously, we added red tracer particles to mark the extension of the initial spot (Fig. 4, right). In all cases one sees that the spot extends about 1 to 1.5 mm further than the initial spot, comparable with the radius of the plaque from a single phage shown in Fig. 1. Remarkably, in all cases we observed lysogenic colonies within the initial spot of infection, in spite of the fact that initially the bacterium was exposed only to about two available phages per host. Comparison of the interior of the three spots confirms the overall expectation that the most lysogenic colonies formed in the wt, fewer formed in the *c*III$^-$ mutant, and the fewest formed in the *c*II$^-$ mutant. However, the structures of the spots are different, as follows. (i) wt spots exhibited a step-like decline in visible colony density moving from the initial spot of phages to the periphery of the spot. Colony frequency within the initial spot was high and homogeneous, whereas no visible new colonies were seen within 0.2 mm from the periphery. (ii) *c*III$^-$ spots contained a 0.3- to 0.5-mm depletion zone, with few colonies just outside the initial spot, followed by double rings of many small colonies halfway between the edge of the initial droplet and the periphery of the spot. When spots were inspected under different conditions, the double ring was not always seen, but we generally observed at least one ring as well as the depletion zone. Consistent with the *c*III$^-$ mutant being less temperate, the outer depleted zone of about 0.4 mm is larger for the *c*III$^-$ mutant than for the wt. (iv) *c*II$^-$ spots sometimes contained a single intermediate ring (not seen on this spot). For some conditions we also observed a depletion zone just inside this ring. As expected, the *c*II$^-$ mutant consistently had fewer lysogens than any of the above phages, and there were no visible colonies within the outer 0.6 mm of the spot.

The most striking difference between the simulation and the experiment is the double ring of the *c*III$^-$ mutant. In particular, it suggests that this mutant sometimes gives more surviving lysogens than the wt.

The spot assay provided a direct measurement of the lysogen frequency, quantified through the final colony number per initial bacterium in the middle of the spot. This method demands that the initial bacterial density is so low that the microcolonies can be counted without overlap (Fig. 5a). The results are summarized in Fig. 5b and c. As expected, we found a higher lysogenic frequency for the wt (~7% at API = 30) than for the *c*III$^-$ (~3% at API = 20) and *c*II$^-$ (~1% at API = 20) mutants. Further, we see that a 10-fold higher API of 200 only moderately increased the lysogen frequency for the phage *c*II$^-$ and *c*III$^-$ mutants. Note that the deduced lysogen frequency is not necessarily the value of α in the model since this decision may depend on the MOI. It should be noted that here we interpret all the survivors in the middle of the spot as lysogens, but some cells may be the transiently immune cells without a properly integrated prophage (CII is known to activate production of the protein needed for integrating λ into the host genome [58]).

Interestingly, the average microcolony volume was inversely proportional to the number of colonies, keeping the total volume of the lysogens per area approximately constant (Fig. 5c). This suggests that the diffusion of nutrients is slow enough that food is simply redistributed between bacteria within the initial phage spot. When lysogenic frequency is low, the smaller number of microcolonies can get more nutrients locally and grow bigger before the nutrients diffuse and are consumed by the sensitive bacteria outside the spot.

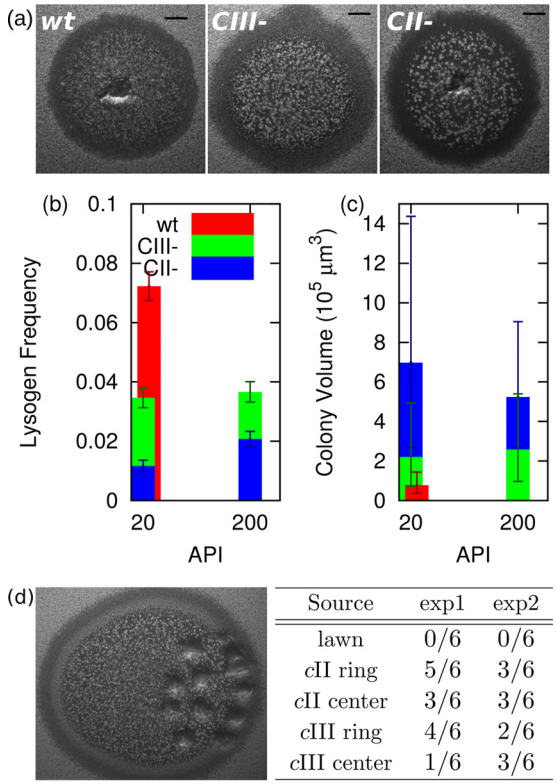

Source	exp1	exp2
lawn	0/6	0/6
*c*II ring	5/6	3/6
*c*II center	3/6	3/6
*c*III ring	4/6	2/6
*c*III center	1/6	3/6

FIG 5 Quantification of the spot assay. (a) Morphology from the spot experiments with the API under the spot at 30 for the wt and 20 for the *c*III$^-$ and *c*II$^-$ mutants. The bottom agar was supplemented with maltose. We use an initial bacterial density of $B_0 = 1/(320\ \mu m^2)$, which is a lower B_0 than that used in the experiment shown in Fig. 4, to minimize colony overlaps for counting. Scale bar, 1 mm. (b) Lysogen frequency is evaluated from (microcolony count in the middle)/B_0 for different API (average phage input) values. (c) Average microcolony volume in the middle, evaluated from the diameter of the colony in the image, assuming that each microcolony is spherical. The error bar for the data in panel b is from the square root of the colony count, and for panel c it shows the standard deviation. (d) Testing lysogenic state in spots. Samples were picked from either the rings or the central region, as shown in the image. Colonies purified from the samples were tested for immunity to λ phage. The results are tabulated to the right, as (number of λ-immune colonies)/(number of tested colonies). In experiment 2 (exp2), the bottom agar was supplemented with maltose.

To determine the composition of microcolonies formed in the spot testing, we picked samples from the rings and central sections of the developed spots (Fig. 5d). Colonies purified from the samples were tested for immunity to λ (see Materials and Methods for details). We found that about half of the bacterial colonies recovered from the spots were λ immune and about half were λ sensitive (Fig. 5d). We failed to observe any λ-resistant colonies but only tested 48 recovered colonies. For the central region, this result suggests that a microcolony may be mixed between lysogens and sensitive bacteria; alternatively, some microcolonies are formed by lysogens and others are formed by bacteria that were infected and the lysogenic pathway was transiently active but the phage failed to integrate in the genome. In the latter case, the phage may provide transient immunity that was lost after some generations. If so, our estimate of lysogen decisions shown in

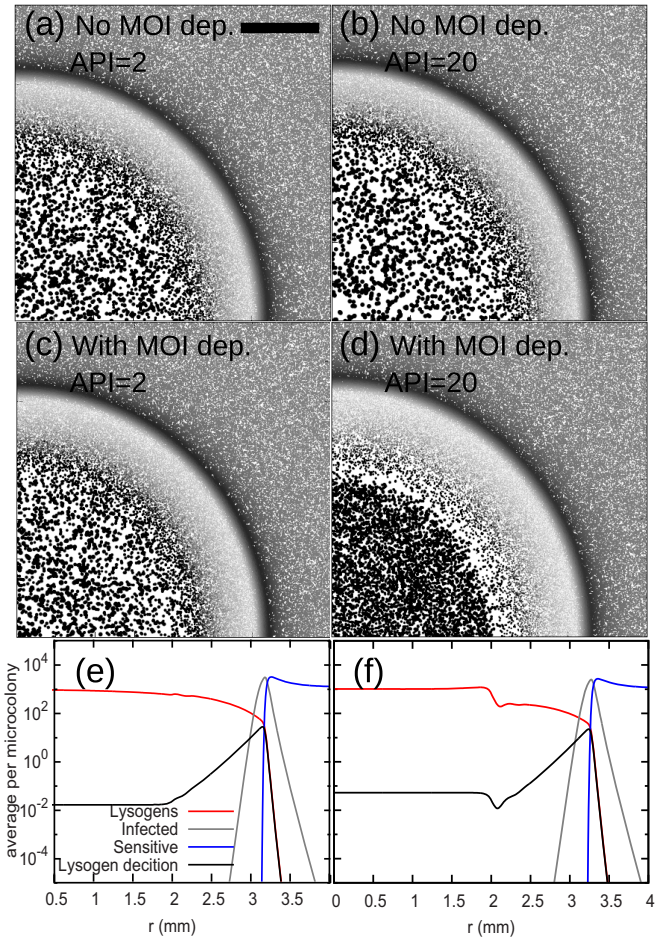

FIG 6 Simulations of spots formed by spot assay. Initial bacterial density is $B_0 = 1/(36\ \mu m^2)$, and images were taken after 10 h of incubation. The area shown has a width of 4 mm, with the middle of the spot being the left bottom corner. The colonies smaller than 10 μm in radius are displayed in a lighter shade of gray in proportion to their radii. The initial spot size is circular, with a radius of 2 mm. For all simulations, $\alpha = 0.01$ was used. (a) Simulation with no MOI dependence and API of 2. (b) Simulation with no MOI dependence and API of 20. (c) Simulation with MOI dependence and API of 2. (d) Simulation with MOI dependence and API of 20. (e) Profiles of lysogens, sensitive cells, infected cells, and number of cells that directly took the lysogen decision (cumulative sum over time) for the simulations with MOI dependence and API of 2. (f) Profiles as described for panel e but for the simulations with MOI dependence and API of 20.

Fig. 5c also counts these incomplete decisions. For the ring region, it could also be that bacteria had already formed a microcolony of a certain size, and then phage may have access to the bacteria closer to the surface, making them into lysogens and leaving sensitive bacteria closer to the center.

Figure 6 shows the simulated spot with an α of 0.01, mimicking the lysogen frequency of the *c*II$^-$ mutant in the experiment shown in Fig. 5. Figure 6a and c show the cases with an API of 2 with and without MOI dependence, respectively. There is little visible difference in the morphologies. However, using an API of 20 in the experiment shown in Fig. 6d, we see that the MOI-dependent simulation can provide an extra ring of depletion just outside the initial spot (Fig. 6d). This is in contrast to the low-API results and to the MOI-independent model (Fig. 6b). Changing α will change the overall surviving microcolony density in the spot, but the spot qualitatively shows the same features.

The depletion regions are apparent in the profile of the density of lysogen decisions per microcolony (Fig. 6f), where one sees a dip just outside the initial spot, at an r_{spot} value of 2 mm. This nonmonotonic behavior is due to the following MOI-dependent mechanism: with a high API, the bacteria under the spot have a high chance to exceed an MOI of 2 and a high probability to form lysogens. However, just outside the spot, the initial density of diffused phage is lower, and the bacteria are mostly infected by an MOI of 1 and thus killed. This makes a disproportionate decrease of bacteria in this narrow region. After the latency period, the phage number increases, and the bacteria that were not killed in the first round divide. Therefore, the ability to form lysogens per microcolony increases. This increase will be stronger as we move toward the periphery of the spot, whereas the region just outside the spot cannot recover because most bacteria are already dead. Noticeably, the model simulation shows that the size of this depletion zone becomes larger if the lysogenic choice demands a higher MOI, e.g., an MOI of >4 (data not shown).

Clearly, the above explanation requires an initial phage density that is high enough to cause an initial MOI of >2 at the spot and killing by diffusion just outside the spot. This explains why the dip does not appear for the low-API case (Fig. 6e). The tendency is also found for a higher α, but the depletion region is then obscured by an excessive number of colonies. Overall, by assuming a high API, we can qualitatively reproduce a bull's-eye-like morphology, but we cannot obtain the morphology of the *c*III$^-$ mutant using the API of 2 from the experiment shown in Fig. 4. Note that the API in the experiment was determined by using PFU counts, which may underestimate the number of phage particles. Extra phage particles may somewhat contribute to the morphology if they help the lysogeny decision under the condition of a high-MOI infection.

We also tried to make α increase with bacterial growth decrease to include the observation of increased lysogenic frequency under slower-growth conditions (32, 33). Since the nutrient decreases with time, this effectively causes a monotonically increasing α with distance from the center and therefore cannot give additional depletion regions (data not shown). Overall, we failed to obtain bull's-eye morphologies with realistic parameters and were unable to obtain the double ring that was observed in some *c*III$^-$ mutant spots (Fig. 4).

DISCUSSION

In spite of its apparent simplicity, the plaque morphology of phage λ is the result of an amazingly complex spatiotemporal process. As the plaque formation progresses, the bacterial lawn changes. At early stages each bacterium is isolated on the lawn, distributed in the top agar, and separated by about 10 to 20 μm from each other when the bacteria are seen from the top. As time progresses, the bacteria grow to form small colonies, and at the same time the available food is depleted while the bacteria gradually enter stationary-phase conditions. This will likely be happening first in the center of colonies that then have reached sizes of the order of 10,000 bacteria. Noticeably, the lysogenic choice should then be favored in this later stage of plaque formation, where cells are growing more slowly (32, 33). At these latter stages one may also have situations where either the λ phage failed to penetrate the entire preformed microcolony or the infections provided some immunity but did not integrate into the chromosome of the bac-

teria. In fact when we tested for the prevalence of bacteria without integrated prophages, we collected bacteria from various regions of the spot for the *c*II$^-$ and *c*III$^-$ mutants and consistently found that about 50% of colonies grown from these isolates were again sensitive to new phage λ infection.

Throughout the early stages of plaque formation, the density of phages is rapidly increasing, and for phage λ this in itself favors the lysogenic choice. As a consequence, the plaque morphology is influenced by the nutritional state of the host, the number of phages that can infect each host, and the fate of phages that become adsorbed in bacteria but cannot complete an infection cycle. The current paper explored part of these dynamics through modeling and observations, thereby highlighting that a turbid plaque is more than just a plaque with a surviving region of lysogens in the middle.

Our simulations demonstrated a number of points, as follows. (i) For a given growth medium, plaque size depends primarily on the phage diffusion constant, second, on the initial bacteria density, and, third, on adsorption rates (varying D_p can change plaque radius by more than a factor of 10, whereas a small adsorption in itself can increase it by 30 to 60%). It should be noted that our diffusion constant D_p may well be smaller than that in pure water since the phage will attach and detach with bacteria, making D_p decrease with the adsorption rate. Experimentally, it has been known that the λ phage with side tail fibers makes plaques with about half the area of those without (38). Existence of side tail fibers affects the adsorption rate by factor 5- to 100-fold (37, 38) and thereby also the effective diffusion constant. It should also be noted that overall results depend on the time scale relative to the maximum growth rate, which we kept constant in the present simulation; changing the growth condition would effectively rescale the relevant rates. We did not alter the latency time in the simulation either, but the latency time should affect the plaque size also (39).

(ii) A temperate phage will have fewer surviving lysogens in the center of plaques than closer to the periphery, and this feature persists even if the phage decision is independent of MOI.

(iii) The visual impression of phage plaques systematically underrepresents lysogens as the field of view moves closer to the periphery of the plaques.

(iv) Plaques from spot assays that show a morphology with high-low-high-low apparent colony density as the field of view moves away from center must have a lysogen decision that depends on MOI. However, absence of such a pattern does not exclude MOI sensitivity.

Experimentally our quantitative analysis highlighted the spot assay, which allowed us to systematically vary the initial number of phages per bacteria in a large homogeneous region of the bacterial lawn. We learned the following. (i) The homogeneous central region provides a direct measurement of lysogen frequency, and this frequency was consistently found to be inversely proportional to the observed colony sizes.

(ii) Many spots for *c*II$^-$ and *c*III$^-$ phages were characterized by a moderate colony density in the central region, surrounded by a high number of smaller colonies and then an apparent clear region in the periphery (data not shown). The wild-type spots typically exhibited a monotonically declining density with distance from center, but under some conditions the wild-type λ phage also exhibited a ring-like morphology.

(iii) For *c*II$^-$ and especially *c*III$^-$ phages at high initial APIs, one often observes a bull's-eye or cocarde morphology (29) with a high central density of surviving colonies and then a depletion region, followed by a high-colony-density region and then finally an apparently clear zone.

Overall, taking into account that bacterial colonies can be too small to be visible, we qualitatively could reproduce the above findings by our simple model. This is remarkable since our model neglected the possibility that an excessive phage load directly kills the bacteria and that bacterial colonies should be more difficult to infect than homogeneously distributed bacteria.

An important quantitative discrepancy between model and experiment is that we only reproduce the bull's-eye morphology when we assume an initial phage number that is in 10- to 100-fold excess of initial bacteria, whereas the pattern was observed in experiments with merely a 2-fold excess. When plaque formation is simulated with a 2-fold excess, the initial infections do not give lysogens. Instead, lysogens form later and more densely as the phages move outwards as the plaque matures. This quantitative disagreement is a challenge to our model.

Another feature that we failed to reproduce is that some *c*III$^-$ spots show a double-ring structure, adding one more features to the bull's-eye morphology [see iii above]). We speculate that this feature is associated with depletion of nutrients, perhaps combined with formation of multiple lysogenic subcolonies within the larger bacterial colonies that are infected in the moderately late stages of plaque formation. Finally, the *c*III$^-$ phages may exhibit MOI sensitivity because they still have CII but at the same time have so little CII that they are not so easily killed by excessive phage load in the later stage of the plaque formation (excessive CII is believed to be poisonous for *E. coli*).

In the present paper, the dynamics of the plaque formation was addressed mainly by the modeling. It will be interesting to follow the time course experimentally, to validate the model, and to deepen our understanding of the dynamics.

Overall, this paper aims to reintroduce plaque morphology as an interesting dynamic system that, in spite of its simplicity, may reveal layers of phage decision strategies and phage-host relationships under various combinations of nutrient ability and phage load per host. For phages in a real ecological environment with spatially structured bacterial populations, our model emphasizes a few important aspects. First of all, the typical killing of the host costs little for the temperate phages compared to the cost for the virulent phages because depletion of nutrients is just delayed until all the available bacteria carry prophages within a plaque. This implies that temperate phages use limited resources in spatially distributed systems more efficiently than virulent ones. Of course, virulent phages are likely to have more free phage particles when plaque formation has stopped, but then the free phages will decay, diffuse away, or be adsorbed to a small number of stationary-phase cells in the periphery of the plaque. If the virulent phages cannot successfully infect stationary-phase cells, then they will have a lower chance of survival than the temperate phages. Second, we found that many bacterial microcolonies are left in stationary phase with incomplete lysogenization. These mixed lysogens may provide an intermediate level of memory where phage could be released when food is again added. This memory allows the phage to survive much longer than in its free form but shorter than in a true lysogen. We speculate that this type of time capsule may also work for some virulent phages that infect bacteria but cannot lyse these in stationary phase.

ACKNOWLEDGMENTS

We thank Sanker Adhya for his inspiration to this project. We also thank Bruce Levin for many constructive comments on the manuscript.

We have no conflicts of interests to declare.

FUNDING INFORMATION

This work, including the efforts of Namiko Mitarai, was funded by Danish National Research Foundation (BASP: DNRF120). This work, including the efforts of Namiko Mitarai, Stanley Brown, and Kim Sneppen, was funded by Danish National Research Foundation (CMoL).

REFERENCES

1. **Whitman WB, Coleman DC, Wiebe WJ.** 1998. Prokaryotes: the unseen majority. Proc Natl Acad Sci U S A **95:**6578–6583. http://dx.doi.org/10.1073/pnas.95.12.6578.
2. **Breitbart M, Rohwer F.** 2005. Here a virus, there a virus, everywhere the same virus? Trends Microbiol **13:**278–284. http://dx.doi.org/10.1016/j.tim.2005.04.003.
3. **Suttle CA.** 2007. Marine viruses—major players in the global ecosystem. Nat Rev Microbiol **5:**801–812. http://dx.doi.org/10.1038/nrmicro1750.
4. **Kamp D, Kahmann R, Zipser D, Broker TR, Chow LT.** 1978. Inversion of the G DNA segment of phage Mu controls phage infectivity. Nature **271:**577–580. http://dx.doi.org/10.1038/271577a0.
5. **Christie GE, Calendar R.** 1990. Interactions between satellite bacteriophage P4 and its helpers. Annu Rev Genet **24:**465–490. http://dx.doi.org/10.1146/annurev.ge.24.120190.002341.
6. **Edgar R, Qimron U.** 2010. The *Escherichia coli* CRISPR system protects from λ lysogenization, lysogens, and prophage induction. J Bacteriol **192:**6291–6294. http://dx.doi.org/10.1128/JB.00644-10.
7. **Labrie SJ, Samson JE, Moineau S.** 2010. Bacteriophage resistance mechanisms. Nat Rev Microbiol **8:**317–327. http://dx.doi.org/10.1038/nrmicro2315.
8. **Makarova KS, Wolf YI, Koonin EV.** 2013. Comparative genomics of defense systems in archaea and bacteria. Nucleic Acids Res **41:**4360–4377. http://dx.doi.org/10.1093/nar/gkt157.
9. **Lwoff A.** 1953. Lysogeny. Bacteriol Rev **17:**269–337.
10. **Stewart FM, Levin BR.** 1984. The population biology of bacterial viruses: why be temperate. Theor Popul Biol **26:**93–117. http://dx.doi.org/10.1016/0040-5809(84)90026-1.
11. **Maslov S, Sneppen K.** 2015. Well-temperate phage: optimal bet-hedging against local environmental collapses. Sci Rep **5:**10523. http://dx.doi.org/10.1038/srep10523.
12. **Dixit PD, Pang TY, Studier FW, Maslov S.** 2015. Recombinant transfer in the basic genome of *Escherichia coli*. Proc Natl Acad Sci U S A **112:**9070–9075. http://dx.doi.org/10.1073/pnas.1510839112.
13. **Waldor MK, Mekalanos JJ.** 1996. Lysogenic conversion by a filamentous phage encoding cholera toxin. Science **272:**1910–1914. http://dx.doi.org/10.1126/science.272.5270.1910.
14. **Brüssow H, Hendrix RW.** 2002. Phage genomics: small is beautiful. Cell **108:**13–16. http://dx.doi.org/10.1016/S0092-8674(01)00637-7.
15. **Waldor MK, Friedman DI.** 2005. Phage regulatory circuits and virulence gene expression. Curr Opin Microbiol **8:**459–465. http://dx.doi.org/10.1016/j.mib.2005.06.001.
16. **Freeman VJ.** 1951. Studies on the virulence of bacteriophage-infected strains of *Corynebacterium diphtheriae*. J Bacteriol **61:**675.
17. **Pappenheimer A, Jr.** 1977. Diphtheria toxin. Annu Rev Biochem **46:**69–94. http://dx.doi.org/10.1146/annurev.bi.46.070177.000441.
18. **Lindsay JA, Ruzin A, Ross HF, Kurepina N, Novick RP.** 1998. The gene for toxic shock toxin is carried by a family of mobile pathogenicity islands in *Staphylococcus aureus*. Mol Microbiol **29:**527–543. http://dx.doi.org/10.1046/j.1365-2958.1998.00947.x.
19. **Jackson MP, Neill RJ, O'Brien AD, Holmes RK, Newland JW.** 1987. Nucleotide sequence analysis and comparison of the structural genes for Shiga-like toxin I and Shiga-like toxin II encoded by bacteriophages from *Escherichia coli* 933. FEMS Microbiol Lett **44:**109–114. http://dx.doi.org/10.1111/j.1574-6968.1987.tb02252.x.
20. **Campbell A.** 1961. Conditions for the existence of bacteriophage. Evolution **2:**153–165.
21. **Levin BR, Stewart FM, Chao L.** 1977. Resource-limited growth, competition, and predation: a model and experimental studies with bacteria and bacteriophage. Am Nat **977:**3–24.
22. **Thingstad TF.** 2000. Elements of a theory for the mechanisms controlling abundance, diversity, and biogeochemical role of lytic bacterial viruses in aquatic systems. Limnol Oceanogr **45:**1320–1328. http://dx.doi.org/10.4319/lo.2000.45.6.1320.
23. **Weitz JS, Hartman H, Levin SA.** 2005. Coevolutionary arms races between bacteria and bacteriophage. Proc Natl Acad Sci U S A **102:**9535–9540. http://dx.doi.org/10.1073/pnas.0504062102.
24. **Haerter JO, Mitarai N, Sneppen K.** 2014. Phage and bacteria support mutual diversity in a narrowing staircase of coexistence. ISME J **8:**2317–2326. http://dx.doi.org/10.1038/ismej.2014.80.
25. **Bull JJ, Vegge CS, Schmerer M, Chaudhry WN, Levin BR.** 2014. Phenotypic resistance and the dynamics of bacterial escape from phage control. PLoS One **9:**e94690. http://dx.doi.org/10.1371/journal.pone.0094690.
26. **Hoyland-Kroghsbo NM, Maerkedahl RB, Svenningsen SL.** 2013. A quorum-sensing-induced bacteriophage defense mechanism. mBio **4:**e00362-12. http://dx.doi.org/10.1128/mBio.00362-12.
27. **Kerr B, Neuhauser C, Bohannan BJ, Dean AM.** 2006. Local migration promotes competitive restraint in a host-pathogen "tragedy of the commons." Nature **442:**75–78. http://dx.doi.org/10.1038/nature04864.
28. **Heilmann S, Sneppen K, Krishna S.** 2012. Coexistence of phage and bacteria on the boundary of self-organized refuges. Proc Natl Acad Sci U S A **109:**12828–12833. http://dx.doi.org/10.1073/pnas.1200771109.
29. **Kaiser AD.** 1955. A genetic study of the temperate coliphage λ. Virology **1:**424–443. http://dx.doi.org/10.1016/0042-6822(55)90036-2.
30. **Clokie MRJ, Kropinski AM (ed).** 2009. Bacteriophages: methods and protocols. I. Isolation, characterization, and interactions. Springer, New York, NY.
31. **Kaiser AD.** 1957. Mutations in a temperate bacteriophage affecting its ability to lysogenize *Escherichia coli*. Virology **3:**42–61. http://dx.doi.org/10.1016/0042-6822(57)90022-3.
32. **Kourilsky P.** 1973. Lysogenization by bacteriophage lambda. Mol Gen Genet **122:**183–195. http://dx.doi.org/10.1007/BF00435190.
33. **Kourilsky P, Knapp A.** 1975. Lysogenization by bacteriophage lambda. III. Multiplicity dependent phenomena occurring upon infection by lambda. Biochimie **56:**1517–1523.
34. **Maynard ND, Birch EW, Sanghvi JC, Chen L, Gutschow MV, Covert MW.** 2010. A forward-genetic screen and dynamic analysis of lambda phage host dependencies reveals an extensive interaction network and a new anti-viral strategy. PLoS Genet **6:**e1001017. http://dx.doi.org/10.1371/journal.pgen.1001017.
35. **Rattray A, Altuvia S, Mahajna G, Oppenheim A, Gottesman M.** 1984. Control of bacteriophage lambda CII activity by bacteriophage and host functions. J Bacteriol **159:**238–242.
36. **Kobiler O, Rokney A, Oppenheim AB.** 2007. Phage lambda CIII: a protease inhibitor regulating the lysis-lysogeny decision. PLoS One **2:**e363. http://dx.doi.org/10.1371/journal.pone.0000363.
37. **Hendrix RW, Duda RL.** 1992. Bacteriophage lambda PaPa: not the mother of all lambda phages. Science **258:**1145–1148. http://dx.doi.org/10.1126/science.1439823.
38. **Gallet R, Kannoly S, Wang N.** 2011. Effects of bacteriophage traits on plaque formation. BMC Microbiol **11:**181. http://dx.doi.org/10.1186/1471-2180-11-181.
39. **Koch AL.** 1964. The growth of viral plaques during the enlargement phase. J Theor Biol **6:**413–431. http://dx.doi.org/10.1016/0022-5193(64)90056-6.
40. **Yin J.** 1991. A quantifiable phenotype of viral propagation. Biochem Biophys Res Commun **174:**1009–1014. http://dx.doi.org/10.1016/0006-291X(91)91519-I.
41. **Yin J, McCaskill J.** 1992. Replication of viruses in a growing plaque: a reaction diffusion model. Biophys J **61:**1540. http://dx.doi.org/10.1016/S0006-3495(92)81958-6.
42. **You L, Yin J.** 1999. Amplification and spread of viruses in a growing plaque. J Theor Biol **200:**365–373. http://dx.doi.org/10.1006/jtbi.1999.1001.
43. **Fort J, Méndez V.** 2002. Time-delayed spread of viruses in growing plaques. Phys Rev Lett **89:**178101. http://dx.doi.org/10.1103/PhysRevLett.89.178101.
44. **Ortega-Cejas V, Fort J, Méndez V, Campos D.** 2004. Approximate solution to the speed of spreading viruses. Phys Rev E Stat Nonlin Soft Matter Phys **69:**031909. http://dx.doi.org/10.1103/PhysRevE.69.031909.
45. **Kaplan DA, Naumovski L, Rothschild B, Collier RJ.** 1981. Appendix: a

model of plaque formation. Gene **13:**221–225. http://dx.doi.org/10.1016/0378-1119(81)90027-5.
46. **Thon G, Bjerling KP, Nielsen IS.** 1999. Localization and properties of a silencing element near the *mat3-M* mating-type cassette of *Schizosaccharomyces pombe*. Genetics **151:**945–963.
47. **Belfort M, Noff D, Oppenheim AB.** 1975. Isolation, characterization and deletion mapping of amber mutations in the cII gene of phage λ. Virology **63:**147–159. http://dx.doi.org/10.1016/0042-6822(75)90380-3.
48. **Miller JH.** 1972. Experiments in molecular genetics, Cold Spring Harbor Laboratory Press, Cold Spring Harbor, NY.
49. **Arber W, Enquist L, Hohn B, Murray NE, Murray K.** 1983. Experimental methods for use with lambda. Cold Spring Harbor Monogr Arch **13:**433–466.
50. **De Paepe M, Taddei F.** 2006. Viruses' life history: towards a mechanistic basis of a trade-off between survival and reproduction among phages. PLoS Biol **4:**e193. http://dx.doi.org/10.1371/journal.pbio.0040193.
51. **Höistad M, Chen KC, Nicholson C, Fuxe K, Kehr J.** 2002. Quantitative dual-probe microdialysis: evaluation of [^{3}H] mannitol diffusion in agar and rat striatum. J Neurochem **81:**80–93. http://dx.doi.org/10.1046/j.1471-4159.2002.00791.x.
52. **Nicholson C, Phillips J.** 1981. Ion diffusion modified by tortuosity and volume fraction in the extracellular microenvironment of the rat cerebellum. J Physiol **321:**225–257. http://dx.doi.org/10.1113/jphysiol.1981.sp013981.
53. **Moldovan R, Chapman-McQuiston E, Wu X.** 2007. On kinetics of phage adsorption. Biophys J **93:**303–315. http://dx.doi.org/10.1529/biophysj.106.102962.
54. **Weitz JS, Mileyko Y, Joh RI, Voit EO.** 2008. Collective decision making in bacterial viruses. Biophys J **95:**2673–2680. http://dx.doi.org/10.1529/biophysj.108.133694.
55. **St-Pierre F, Endy D.** 2008. Determination of cell fate selection during phage lambda infection. Proc Natl Acad Sci U S A **105:**20705–20710. http://dx.doi.org/10.1073/pnas.0808831105.
56. **Avlund M, Dodd IB, Sneppen K, Krishna S.** 2009. Minimal gene regulatory circuits that can count like bacteriophage lambda. J Mol Biol **394:**681–693. http://dx.doi.org/10.1016/j.jmb.2009.09.053.
57. **Avlund M, Dodd IB, Semsey S, Sneppen K, Krishna S.** 2009. Why do phage play dice? J Virol **83:**11416–11420. http://dx.doi.org/10.1128/JVI.01057-09.
58. **Katzir N, Oppenheim A, Belfort M, Oppenheim AB.** 1976. Activation of the lambda *int* gene by the *c*II and *c*III gene products. Virology **74:**324–331. http://dx.doi.org/10.1016/0042-6822(76)90339-1.
59. **Ptashne M.** 2004. A genetic switch: phage lambda revisited, 3rd ed. Cold Spring Harbor Laboratory Press, Cold Spring Harbor, NY.
60. **Kobiler O, Rokney A, Friedman N, Stavans J, Oppenheim AB.** 2005. Quantitative kinetic analysis of the bacteriophage λ genetic network. Proc Natl Acad Sci U S A **102:**4470–4475. http://dx.doi.org/10.1073/pnas.0500670102.
61. **Oppenheim AB, Kobiler O, Stavans J, Court DL, Adhya S.** 2005. Switches in bacteriophage lambda development. Annu Rev Genet **39:**409–429. http://dx.doi.org/10.1146/annurev.genet.39.073003.113656.
62. **Wang I-N, Smith DL, Young R.** 2000. Holins: the protein clocks of bacteriophage infections. Annu Rev in Microbiology **54:**799–825. http://dx.doi.org/10.1146/annurev.micro.54.1.799.
63. **Trusina A, Sneppen K, Dodd IB, Shearwin KE, Egan JB.** 2005. Functional alignment of regulatory networks: a study of temperate phages. PLoS Comput Biol **1:**e74. http://dx.doi.org/10.1371/journal.pcbi.0010074.
64. **Rothenberg E, Sepúlveda LA, Skinner SO, Zeng L, Selvin PR, Golding I.** 2011. Single-virus tracking reveals a spatial receptor-dependent search mechanism. Biophys J **100:**2875–2882. http://dx.doi.org/10.1016/j.bpj.2011.05.014.